Quasi-phase-matched $\chi^{(3)}$-parametric interactions in sinusoidally tapered waveguides

Mohammed F. Saleh
Institute of Photonics and Quantum Sciences, Heriot-Watt University, EH14 4AS Edinburgh, United Kingdom and Department of Mathematics and Engineering Physics, Alexandria University, Alexandria, Egypt

(Received 15 September 2017; revised manuscript received 24 November 2017; published 29 January 2018)

In this article, I show how periodically tapered waveguides can be employed as efficient quasi-phase-matching schemes for four-wave mixing parametric processes in third-order nonlinear materials. As an example, a thorough study of enhancing third-harmonic generation in sinusoidally tapered fibers has been conducted. The quasi-phase-matching condition has been obtained for nonlinear parametric interactions in these structures using Fourier-series analysis. The dependencies of the conversion efficiency of the third harmonic on the modulation amplitude, tapering period, longitudinal-propagation direction, and pump wavelength have been studied. In comparison to uniform waveguides, the conversion efficiency has been enhanced by orders of magnitudes. I envisage that this work will have a great impact in the field of guided nonlinear optics using centrosymmetric materials.

DOI: 10.1103/PhysRevA.97.013850

I. INTRODUCTION

Optical parametric nonlinear processes have been intensively harnessed in applications such as optical-frequency conversion, amplification, and oscillation [1]. Efficient parametric wave-mixing processes in nonlinear media are inherently constrained by energy and momentum conservation. The latter is known as the phase-matching condition. Two techniques have been successfully employed to satisfy this condition in second-order nonlinear media. The first technique is based on interaction between non-collinear propagating photons in birefringent materials [2]. In the second technique, known as quasi-phase-matching (QPM), the nonlinear coefficient $\chi^{(2)}$ is longitudinally modulated with a specific period [3]. Using periodically poled ferroelectric crystals, where the nonlinear coefficient can be flipped every half this period, this method has been experimentally demonstrated nearly after two decades from its proposal due to the lack of the suitable fabrication facilities at that time [4]. QPM structures have remarkably boosted the classical and quantum optical nonlinear-frequency-conversion applications in bulk and integrated structures [5,6]. This technique enables, for instance: (i) Collinear interactions between copolarized waves results in exploiting the strongest component of the second-order nonlinear tensor; (ii) on-chip nonlinear interactions that lead to efficient and scalable optical integrated devices [7]; (iii) tailoring the spectral properties of the output photons via engineering the poling pattern [8].

In third-order $\chi^{(3)}$-nonlinear media, few techniques have been used to satisfy the inherent difficult phase matching condition associated with four-wave mixing parametric processes. For instance: (i) Spontaneous four-wave mixing in waveguides, in which two photons will coalesce to generate two other photons, has been enabled via balancing the waveguide and material dispersion in narrow spectral range near the zero dispersion wavelength, or exploiting the nearly phase-matched range, where the coherence length is much longer than the structure length [9–12]. (ii) Third-harmonic generation has been enhanced via nonlinear interactions in multimode waveguides [13–15], using a hybrid photonic crystal fibre to allow interaction between a pump wave with its third-harmonic, both in the fundamental mode [16] and exploiting slow-light effect introduced by photonic crystals [17].

Having robust $\chi^{(3)}$-QPM platforms would push four-wave mixing parametric processes to a new regime, such as on-demand spontaneous four-wave mixing process, and efficient sum-frequency generation, where three different photons combine together to generate a photon at their sum frequency, with all the photons in the fundamental mode. The inverse of the latter process, where one photon splits into three correlated or entangled photons "photon triplets," can also take place. Having an efficient triplet source is beneficial for quantum-secret sharing applications [18,19], as well as, building large-scale silicon-photonic quantum computers [20]. Few different QPM techniques in $\chi^{(3)}$-media have been proposed and implemented for parametric amplification, third-harmonic generation, and controlling modulation instability, such as cascaded stages made of a dispersion-shifted fiber and a single-mode uniform fibre [21], ultrasound waves in gas cells [22], counter-propagating train of pulses [23], and sinusoidally tapered fibres and silicon nanowires [24–29].

Periodically tapered-waveguides (PTWs) technique is a potential route to achieve robust $\chi^{(3)}$-QPM platforms, analog to periodic poling, since by only longitudinally engineering the waveguide cross-section the phase-matching condition could be satisfied. This technique is currently hurdled by fabrication methods that limits the tapering period to the millimeter and submillimeter range in silicon nanowires [25]. In addition, a careful analysis is essential to understand how simultaneous longitudinal variations of both linear and nonlinear properties of the waveguide modify the well-known QPM condition in periodically poled structures. In this article, I will explain using Fourier-series analysis how PTWs could act as an efficient analog to QPM schemes in $\chi^{(3)}$-nonlinear media for enhancing third harmonic (TH) generation, as an example of four-wave mixing parametric processes.

The article is organized as follows: The model and the governing equations have been introduced in Sec. II. Section III discusses the mechanism of satisfying the phase matching condition in PTWs. Section IV is devoted for discussions and future work. Finally, my conclusions are summarized in Sec. V.

II. GOVERNING EQUATIONS OF THIRD-HARMONIC GENERATION IN PERIODICALLY TAPERED WAVEGUIDES

Consider a TH parametric process in a single-mode PTW with a tapering period Λ_T. A piecewise model has been developed to study this process in this type of waveguides, however, in general it could be applied for any other parametric processes. The procedure is the following: (i) Use Maxwell equations and assume that $|\partial_z \beta_i| \ll \beta_i^2$, where z is the longitudinal direction, and β_i is the propagation constant of a wave i. (ii) Discretize the waveguide into infinitesimal segments, where the waveguide cross-section is assumed to be constant. An eigenvalue problem can be solved to determine the fundamental mode profile and its propagation constant. (iii) Apply the slowly varying envelope approximation, the interaction between a fundamental pump wave and its TH in the limit of CW-approximation inside each segment is governed by [9]

$$\begin{aligned}\partial_z U_1 &= j[\gamma_{1111}|U_1|^2 + 2\gamma_{1133}|U_3|^2]U_1 \\ &\quad + j\gamma_{1113}U_3U_1^{*2}e^{j\Delta\phi(z)}, \\ \partial_z U_3 &= j[\gamma_{3333}|U_3|^2 + 2\gamma_{3311}|U_1|^2]U_3 \\ &\quad + j\tfrac{1}{3}\gamma_{3111}U_1^3 e^{-j\Delta\phi(z)},\end{aligned} \tag{1}$$

where U_1 and U_3 are the complex envelopes of the fundamental and TH waves, respectively, $\Delta\phi = \int_0^z \Delta\beta(z')dz'$ is the phase mismatching, $\Delta\beta = \beta_3 - 3\beta_1$ is the propagation-constant mismatching, $\beta_i = n(\omega_i)\omega_i/c$, ω is the angular frequency, n is the linear refractive index, c is the speed of light, $\gamma_{ijkl} = n_2\omega_i/cA_{\text{eff}}^{(ijkl)}$, n_2 is the nonlinear refractive index in units m^2/W, $A_{\text{eff}}^{(ijkl)}$ is the effective area [30],

$$A_{\text{eff}}^{(ijkl)} = \frac{\sqrt{\prod_{u=i,j,k,l}\iint dxdy\,\psi_u^2(x,y)}}{\iint dxdy\prod_{u=i,j,k,l}\psi_u(x,y)}, \tag{2}$$

x and y are the transverse coordinates, and ψ_i is the transverse profile of wave i. (iv) Solve the differential equations in each segment in the regime of undepleted-pump approximation, the conversion efficiency of the TH can be written as

$$\Gamma_{\text{THG}}(z) = \frac{1}{9}P_i^2\left|\int_0^z dz\;\gamma_{3111}(z)\;e^{j[3\gamma_{1111}P_i z - \Delta\phi(z)]}\right|^2, \tag{3}$$

with $P_i = |U_1(0)|^2$ is the input power. If $\Delta\beta$ *were* spatial-independent, a periodic modulation of γ_{3111} could be used directly to correct the phase mismatching similar to QPM techniques in $\chi^{(2)}$-nonlinear media. It is worth noting that in tapered waveguides the phase mismatching $\Delta\phi$ at any waveguide segment is related to the preceding segments, because of the integration that always runs from the beginning of the waveguide [31]. Assuming plane-waves solutions in tapered waveguides could lead to pitfalls since $\Delta\beta$ varies along the structure. To measure the enhancement of the conversion efficiency using this technique, the quantity

$$\Upsilon = \Gamma_{\text{THG}}/\,\Gamma_{\text{THG}}^{\text{UNI}}, \tag{4}$$

is introduced, where $\Gamma_{\text{THG}}^{\text{UNI}}$ is the maximum conversion efficiency obtained using a uniform waveguide with an average transverse dimensions.

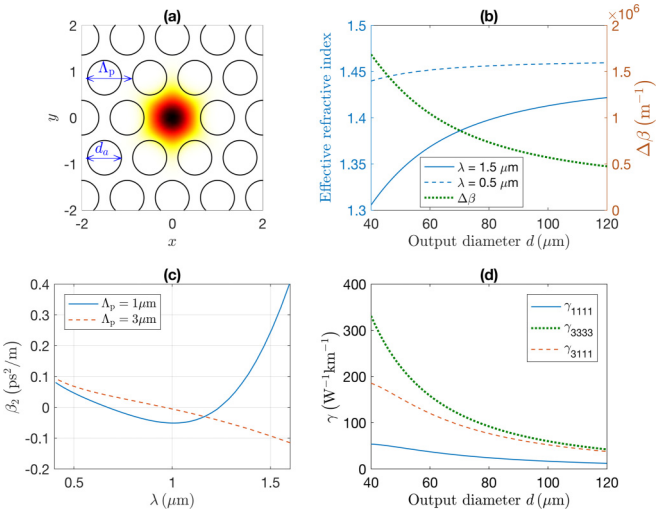

FIG. 1. Linear and nonlinear properties of a silica solid-core DOF with Λ_p varies between 1 and 3 μm, a hole-diameter $d_a = 0.75\Lambda_p$, an output-diameter $d = 40\Lambda_p$, and $n_2 = 2.25 \times 10^{-20}$ m^2/W. The wavelength λ of the pump and TH waves are 1.5 and 0.5 μm. (a) The fundamental-mode transverse profile of the TH at $\Lambda_p = 1\,\mu$m. (b) The dependence of the effective refractive indexes and propagation-constant mismatching $\Delta\beta$ on the output diameter. (c) The wavelength dependence of the second-order dispersion coefficient β_2. (d) The dependence of the nonlinear coefficients γ on the output diameter. These parameters will be used in the subsequent simulations presented in this paper, unless stated otherwise.

Without loss of generality, I have used in simulations the parameters of dispersion oscillating fibers (DOFs), which are silica solid-core sinusoidally tapered microstructured fibers, exploited in controlling modulation instability [26–29]. The fiber output diameter d is given by

$$d(z) = d_{\text{av}}[1 - \Delta d\,\cos(2\pi z/\Lambda_T)], \tag{5}$$

where d_{av} is the average diameter, and Δd is the amplitude of modulation. The linear and nonlinear properties of a DOF with an outer diameter d that varies sinusoidally with $d_{\text{av}} = 80\,\mu$m, and $\Delta d = 0.5$ is shown in Fig. 1. The fiber is made of a stack of hollow capillary tubes with a pitch Λ_p varies between 1 and 3 μm and a hole-diameter $d_a = 0.75\Lambda_p$. The mode profile of the TH at the smallest diameter is displayed in Fig. 1(a), assuming a pump source with wavelength $\lambda = 1.5\,\mu$m. The dependency of the effective refractive index of the fundamental and TH on d, and the corresponding $\Delta\beta$ are shown in Fig. 1(b). The simulations are performed using "COMSOL," a commercial finite-element method, including material dispersion of silica [1]. The maximum fiber guiding loss is less than 0.1 dB/m. The fiber second-order dispersion

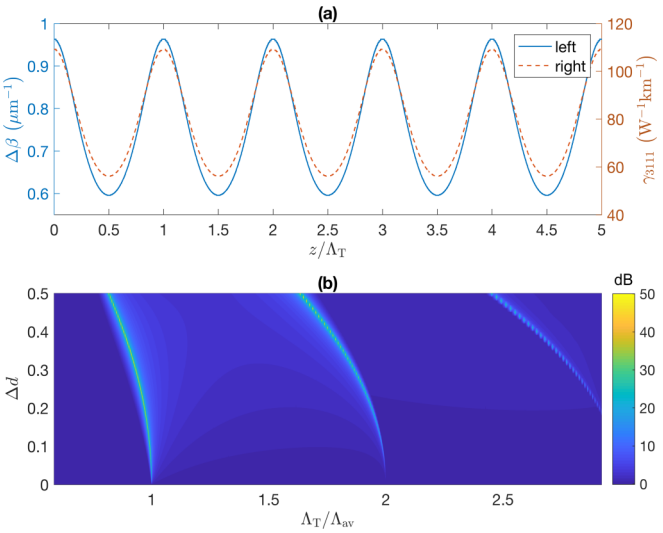

FIG. 2. (a) Spatial dependence of $\Delta\beta$ and γ_{3111} in a DOF used in Fig. 1 with $d_{av} = 80\,\mu$m and $\Delta d = 0.2$. (b) Dependence of Υ on the tapering period Λ_T and modulation amplitude Δd after propagating 1000 periods, with $\Lambda_{av} = 8.56\,\mu$m.

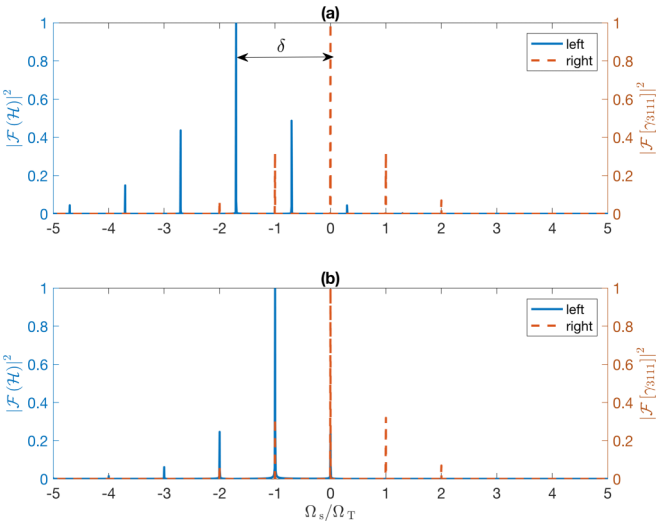

FIG. 3. Power spectral densities of $\mathcal{H}$ and γ_{3111} in a DOF with $d_{av} = 80\,\mu$m and $\Delta d = 0.4$, (a) $\Lambda_T/\Lambda_{av} = 1.5$, (b) $\Lambda_T/\Lambda_{av} = 0.88$. $\mathcal{F}$ is the Fourier-transform operator.

coefficient β_2 dependence on the wavelength at the minimum and maximum of Λ_p is displayed in Fig. 1(c). The TH wave is always in the normal dispersion regime, while the fundamental wave shifts continuously along the fiber between the normal and anomalous dispersion regimes. Figure 1(d) presents the dependencies of some of the nonlinear coefficients γ_{ijkl} on d. The strong modulation of d results in variation of γ_{3111} between 37.8 and 185.5 W^{-1}km^{-1}. The nonlinear phase contribution to TH, $3\gamma_{1111}P_i$, in Eq. (3) is safely neglected in this work, since it requires at least a megawatt CW pump source to be comparable to $\Delta\beta$. I have used in the simulations presented in the paper the parameters of this fiber, however, with different Δd. Numerical integrations should be performed with step size much smaller than the tapering period to avoid accumulation of computational errors. For a Gaussian pulse with 1 ps temporal duration and 1 W input power, modulation instability takes place roughly after more than 10 meters of propagation [9].

III. QUASI-PHASE-MATCHING MECHANISM IN SINUSOIDALLY TAPERED WAVEGUIDES

Unlike QPM in $\chi^{(2)}$-nonlinear media, both the nonlinear coefficient γ_{3111} and the propagation-constant mismatching $\Delta\beta$ are periodically varying in a DOF, as depicted in Fig. 2(a). $\Delta\beta(z) = \Delta\beta_m + \Delta\beta_w(z)$, where $\Delta\beta_m$ and $\Delta\beta_w$ are the material and waveguide mismatchings, respectively. $\Delta\beta_w$ has its strongest (weakest) value at the smallest (largest) fiber diameter. Hence, $\Delta\beta$ can be approximately written as

$$\Delta\beta = \Delta\beta_{av}[1 + \Delta d\,\cos(\Omega_T z)], \tag{6}$$

where $\Delta\beta_{av}$ is the average value of $\Delta\beta$, and $\Omega_T = 2\pi/\Lambda_T$ is the tapering spatial frequency. There is a range of values of $\Delta\beta$ for a single nonlinear parametric process, because of the periodic modulation of the fiber cross-section area. The corresponding phase mismatching can be written in analog to uniform waveguides as $\Delta\phi = \widetilde{\Delta\beta} z$, $\widetilde{\Delta\beta} = \Delta\beta_{av}[1 + \Delta d\,\mathrm{sinc}(\Omega_T z)]$, and $\mathrm{sinc}(x) = \sin(x)/x$. After a long propagation, $\widetilde{\Delta\beta}$ tends to $\Delta\beta_{av}$.

The novelty of this research is in obtaining the right QPM conditions that allow a DOF (or in general a PTW) to be employed as an efficient $\chi^{(3)}$-QPM structure. Figure 2(b) shows the right combination of the tapering period and the amplitude of modulation that leads to strong enhancement ($\lesssim$50 dB) of TH generation in comparison to a uniform waveguide with the same length. The tapering period is normalized to $\Lambda_{av} = 2\pi/\Delta\beta_{av}$. The right Λ_T is close to Λ_{av}; however, it starts to deviate as Δd increases. This matches with the sinc-dependence of $\widetilde{\Delta\beta}$. In PTWs, the harmonics of the nonlinear coefficients will be used to correct a modified value $\Delta\beta_{av}$ that averages the phase mismatching accumulated during the positive and negative halves of the sinc-function. The bright trajectories shown in the plot corresponds to the fundamental period and its multiples. Interestingly, even for small modulation 1–2%, Υ or Γ_{THG} could be dramatically enhanced. For higher multiples, the enhancement drops and a stronger amplitude modulation is needed. $\Delta\beta_{av}$ is large in the range of 10^6 for TH, which suggests a tapering period in the micrometer regime. Using Fig. 1(b), the condition $|\partial_z\beta_i| \ll \beta_i^2$ is still satisfied by approximately 2 order of magnitudes for this range of tapering periods.

The power-spectral densities of γ_{3111} and $\mathcal{H} = \exp[-i\Delta\phi]$ are plotted versus the spatial frequency Ω_s, normalized to Ω_T, in Figs. 3(a) and 3(b). The Fourier spectrum of γ_{3111} is symmetric with a zero-component and multiples of Ω_T. Interestingly, I found that the Fourier spectrum of $\mathcal{H}$ is similar to that of γ_{3111}; however, it is shifted to the left with multiples of another spatial frequency Ω_T'. The strength of the sidebands of both spectra increases with Δd and are rapidly decaying for higher-order components. Hence, the integrand in Eq. (3) can be written using the Fourier series as

$$\gamma_{3111}\mathcal{H} = \sum_p \tilde{\gamma}_p e^{jp\Omega_T z} \sum_q \tilde{h}_q e^{jq\Omega_T z - j\delta z}, \tag{7}$$

where $\delta = \Omega_T - \Omega'_T$ depends on the tapering period and the amplitude of modulation, $\tilde{\gamma}_p$ and $\tilde{h}_q$ are the Fourier coefficients of γ_{3111} and $\mathcal{H}$, respectively, and $p,q = 0, \pm 1, \pm 2, \ldots$. When δ is zero or $m\Omega_T$ with m an integer, the power spectral densities of γ_{3111} and $\mathcal{H}$ will coincide, as depicted in Fig. 3(b).

In periodically poled waveguides, there is a single phase-mismatching Fourier component that will be counteracted by one of the harmonics of the periodic nonlinear coefficient by choosing the right poling period. Whereas in PTWs, there are multiples of phase mismatchings components with spatial frequencies $q\Omega_T - \delta$. However, if $\delta = m\Omega_T$, Eq. (7) can be rewritten as

$$\gamma_{3111}\mathcal{H} = \sum_p \tilde{\gamma}_p e^{jp\Omega_T z} \sum_{q'} \tilde{h}_{q'} e^{jq'\Omega_T z}, \tag{8}$$

with $q' = q - m$. In this case, multiple opposite combinations of (p,q') such as $(0,0), (1,-1), (-1,1), (-2,2), (2,-2)\ldots$ will be exploited simultaneously to correct the phase mismatching introduced by the periodic nature of the waveguide. A Fourier component of γ_{3111} will balance a component of $\mathcal{H}$ that has an opposite spatial frequency. Hence, the QPM condition for these combinations is

$$G_{p,q'} = p\Omega_T + q'\Omega_T = 0. \tag{9}$$

By proper adjustment of both Λ_T and Δd, this condition is satisfied and dramatic enhancement of TH generation is achieved as displayed in Fig. 2(b). Deviating from the perfect QPM condition of the PTWs results in deteriorating the conversion efficiency. The spectrum $|\mathcal{F}(\mathcal{H})|^2$ continues to shift to the left as Λ_T increases. Hence, Υ or Γ_{THG} starts to drop for higher values of Λ_T due to a weakly overlap between the strong spectral components of γ_{3111} and $\mathcal{H}$. This can be recovered via using longer waveguides, materials with large effective nonlinearity, or large input power.

The conversion efficiency can be rewritten as

$$\Gamma_{THG}(z) = \frac{1}{9} P_i^2 z^2 \left| \sum_{p,q'} \tilde{\gamma}_p \tilde{h}_{q'} \mathrm{sinc}(G_{p,q'} z/2) e^{jG_{p,q'} z/2} \right|^2, \tag{10}$$

using Eq. (8). Therefore, Γ_{THG} depends on a superposition of multiple sinc functions, modulated with different complex amplitudes and relative phases. Figures 4(a) and 4(b) depict the spatial dependence of Υ over short and long propagation distances. For comparison, the spatial dependence of Υ in a uniform waveguide and when Δd does not equal to the right value are also shown in Fig. 4(a). Opposite combinations with $p + q' = 0$ leads to a quadratic spatial dependence and the growth of Γ_{THG}. Contrarily, other combinations that do not satisfy the QPM condition, Eq. (9), such as $(0,-1)$, $(0,1)$, $(0,-2)$, $(-2,1)$..., results in a sinusoidal behavior and does not contribute to the growth of the the conversion efficiency. The strongest dominant component of these combinations is $G_{0,-1}$, as shown in Fig. 3(b).

On a macroscopic scale, $z \ll 1/|G_{0,-1}|$, Γ_{THG} has the classical quadratic spatial dependence. Afterwards, Γ_{THG} starts to sinusoidally oscillates and approaches zero on an intermediate scale, when z is multiples of $2\pi/|G_{0,-1}|$. An overall gain can be obtained after long propagation if the amplification due

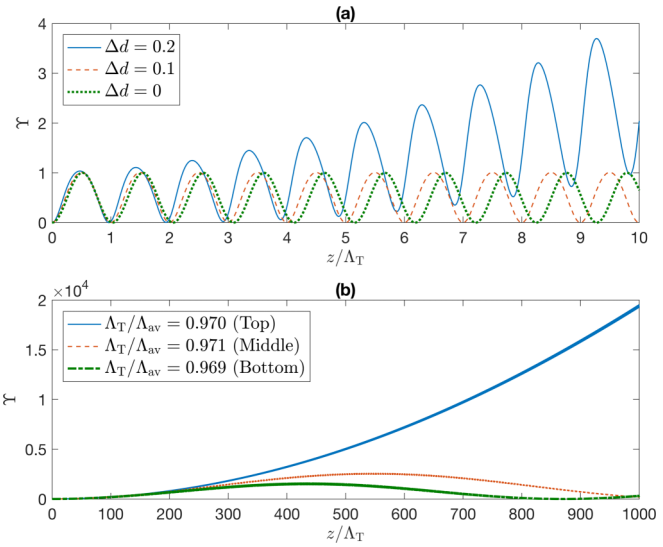

FIG. 4. Spatial dependence of Υ in a DOF with $d_{av} = 80\,\mu$m, and $P_i = 1$ W. (a) Short scale with $\Delta d = 0, 0.1, 0.2$, and $\Lambda_T/\Lambda_{av} = 0.97$. (b) Long scale with $\Delta d = 0.2$, and $\Lambda_T/\Lambda_{av} = 0.97, 0.971, 0.969$.

to the (p,q') opposite combinations overcomes the sinusoidal oscillation due to $G_{0,-1}$ component within each period, as displayed in Fig. 4(b) (solid-blue curve). The result would behave as an amplified sinusoidal wave.

In PTWs, there is a coherence length $l_c^{(s)} = 2\pi/|G_{0,-1}|$ that corresponds to the short-scale sinusoidal oscillations. There is also another long-scale coherence length $l_c^{(l)}$ due to the non-ideal compensation of the phase mismatching, $l_c^{(l)} = 2\pi/|G_{p,q'}|$, with $(p,q') = (0,0)$ or $(1,-1)$. These are the two strongest Fourier components that lead to the growth of the TH. For perfect alignment between the spectra of γ_{3111} and $\mathcal{H}$, $G_{0,0} = G_{-1,1} = 0$, and $l_c^{(l)}$ goes to infinity. As shown in Fig. 4(b), Υ is reduced by approximately an order of magnitude by slight change of Λ_T. For the first 200–300 periods of propagation, Υ is approximately the same for the three values of Λ_T. Afterwards, it decays for the nonideal values of Λ_T due to the accumulation of the phase-mismatching. Fine tuning is necessary for long propagation, similar to periodic poling technique [5], since the linewidth of the Fourier components of γ_{3111} and $\mathcal{H}$ becomes very sharp as the structure length increases. This restricts the values of Λ_T and Δd to allow an alignment between the two spectra. The fine tuning is relaxed for higher values Δd as depicted by a broadening of the bright trajectories in Fig. 2(b).

The dependence of the conversion efficiency on the pump wavelength at the end of a waveguide with length L is depicted in Fig. 5. Figure 5(a) displays the case in which one pump photon frequency is fixed at $1.5\,\mu$m, whereas the frequencies of the other two photons are scanned around that value, such that the TH is $0.5\,\mu$m. Using Eq. (10), only terms with $G_{p,q'} \approx 0$ will contribute to the output spectrum at a fixed length. Hence, Γ_{THG} will behave as a squared sinc-function with weak sidelobes, and spectral bandwidth that is inversely proportional to L, as demonstrated in Fig. 5(a). Figures 5(b) and 5(c) show the 2D representation of Γ_{THG} (equivalent to the phase-matching function of photon triplets [15,16]) over which the energy and momentum conservation conditions are

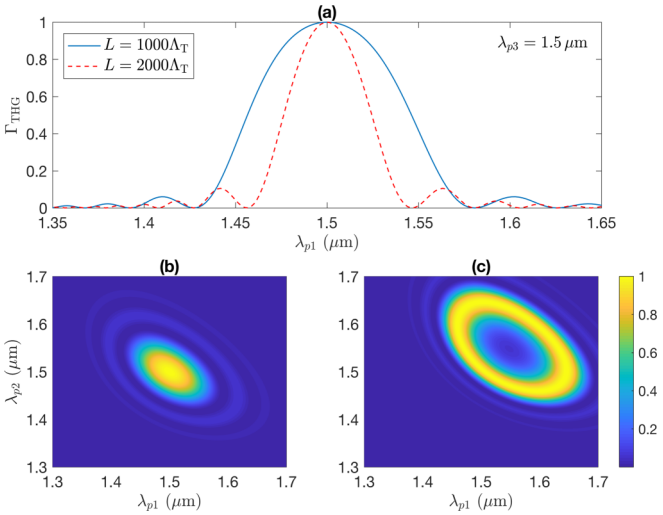

FIG. 5. Wavelength-dependence of the normalized conversion efficiency of the TH generation at the end of a DOF with $d_{av} = 80\,\mu$m, $\Delta d = 0.2$, $\Lambda_T/\Lambda_{av} = 0.97$, and $P_i = 1$ W. $\lambda_{p1}, \lambda_{p2}, \lambda_{p3}$ are the three pump photons at and around the fundamental frequency $1.5\,\mu$m. (a) 1D representation with the TH at 500 nm. (b, c) 2D representation with the TH at 500 and 516 nm, respectively, and $L = 1000\Lambda_T$.

satisfied for TH at 500 and 516 nm, respectively. The spectrum maintains the feature of having a single main lobe over a relatively broad range of a TH between 500 ± 10 nm.

IV. DISCUSSIONS AND FUTURE WORK

In this section, I will discuss some of the potential applications, challenges, and required future work to employ PTWs as full analogues of periodically poled microstuctures for classical and quantum third-order nonlinear parametric process.

Single-photons that are vital for photonic-based quantum information science could be generated, for instance, via the opposite parametric process of TH generation since both share the same phase-matching condition [15]. In this case, one pump photon can split into three downconverted photons results in photon-triplets. Correlations between the photon triplets should be minimized to increase the spectral purity of the single photons, for them to be useful in quantum applications. The spectral purity of single photons depends on the phase-matching contour plots, displayed in Figs. 5(b) and 5(c), and the pump envelop profile, which is neglected in this work assuming CW operation. Minimizing the spectral correlations can be obtained by orienting the phase matching function at specific degrees to allow group-velocity matching between the mother and daughter photons together with the phase-matching. This is an interesting point of research that goes beyond the scope of this paper and requires further future investigation. Even under group-velocity matching, the spectral purity may still be limited by spurious frequency correlations due to the sidelobes of the phase-matching sinc-function. However, obtaining relatively high spectral-purity single photons in PTWs is anticipated because of the weakness of the sidelobes, shown in Fig. 5.

Using tapered single-mode waveguides can lead to a power loss due to coupling of the fundamental mode with higher-order cladding modes. This would impose an additional condition on the acceptable values of Δd and Λ_T that can ensure an *adiabatic propagation* inside PTWs with minimal losses. Using the weak-power-transfer criterion [31,32], the condition that delineates between adiabatic and lossy tapering regimes can be written as

$$\alpha = \left| \frac{\sigma(z)\lambda}{2n_{\max}\left[n_a^2(z) - n_b^2(z)\right]} \frac{dr}{dz} \right| \ll 1, \tag{11}$$

where $n_{\max}$ is the maximum core refractive index, a,b refers to the fundamental mode and the closest higher-order cladding mode, n_i is the local effective refractive index of mode i, σ is the overlap integral of the two mode profiles with the radial-derivative of the refractive index transverse distribution,

$$\sigma(z) = \frac{\tilde{\sigma}(z)}{r_{av}} = \frac{1}{r_{av}} \frac{\iint d\rho d\theta\, \psi_a \psi_b \frac{dn^2}{d\rho}}{\sqrt{\iint d\rho d\theta\, \psi_a^2 \iint d\rho d\theta\, \psi_b^2}}, \tag{12}$$

$\tilde{\sigma}$ is the normalized overlap integral, r_{av} is the average fiber radius, the field distribution ψ is defined in the polar coordinates r and θ, r is the radial distance, θ is the azimuthal angle, and $\rho = r/r_{av}$. For PTWs, substituting $r = r_{av}[1 - \Delta d \cos(2\pi z/\Lambda_T)]$, Eq. (11) becomes

$$\alpha = \left| \frac{\pi\tilde{\sigma}\lambda\Delta d \sin(2\pi z/\Lambda_T)}{n_{\max}\Lambda_T\left(n_a^2 - n_b^2\right)} \right| \ll 1. \tag{13}$$

Hence, small amplitude of modulation and large tapering period is required to allow for adiabatic propagation, as intuitively expected. A full analysis of the above criterion requires numerical calculations of all the modes of the system along a length of at least a half tapering period with very small increments, which will be subject for future studies. However, estimated values of α could be determined for the proposed structure of TH generation. Both $\tilde{\sigma}$ and $n_a^2 - n_b^2$ slightly change along the waveguide. Hence, the adiabatic criterion will depend on the sine term that reaches its maximum unity when z is odd multiple numbers of $\Lambda_T/4$. This corresponds to the positions where the fiber radius equals to its average value. The estimated maximum value of α at these positions is ≈ 0.2 assuming $\lambda = 0.5\,\mu$m, $\tilde{\sigma} = 0.5$, $n_{\max} = 1.45$, $n_a = 1.44$, and $n_b = 1.43$, $\Delta d = 0.1$, and $\Lambda_T = 8.5\,\mu$m. So, the criterion is moderately satisfied at and around these positions. However, when z is multiples of $\Lambda_T/2$, the criterion is completely satisfied. Therefore, to avoid accumulation of nonadiabatic losses, a structure with a smaller Δd [as shown in Fig. 2(b)], suppressed lossy higher-order cladding modes, or a careful designed waveguide length should be used.

The possible longest tapering period required to obtain high Γ_{THG} is approximately few tens of microns using Fig. 2(b), which is currently unaccessible via the current DOF fabrication technology. Currently, the state-of-the-art of DOF fabrication is limited to a period of few tens of centimeters over about 200 m long [28,29]. However, with the rapid progress in the fabrication methods and via using advanced post-treatment processes, I would imagine that this limitation will be mitigated

in the future. Alternatively, these estimated tapering periods could be realized sooner using other waveguide platforms such as laser-written and planar waveguides [33,34], which are more promising techniques and will be considered in future investigations as potential candidates for experimental demonstration. In fact, width-modulated sinusoidal tapering with 1-mm period has been demonstrated in high-nonlinear rectangular silicon nanowires over 5 mm long using e-beam lithography [25]. Also in these platforms, temperature-tuning effect [35,36] can be utilized to correct any phase-mismatching introduced by fabrication tolerance via integrating thermo-optic switches. Periodically poled $\chi^{(2)}$-QPM microstructures were demonstrated after two decades of their proposal. So, one could anticipate that on-demand PTWs will be available within the same period, or may be even less.

V. CONCLUSIONS

In conclusion, I have theoretically demonstrated the concept of having efficient QPM schemes in third-order nonlinear materials using periodically tapered waveguides. In this paper, I have studied as an example enhancing third-harmonic generation in longitudinally sinusoidally tapered fibers. However, the study is applicable for other FWM processes such as parametric amplification, where the phase mismatching is relatively arbitrary and the corresponding tapering period can be set by the current fabrication technologies. In these structures, there are multiple values of the phase mismatching of a single nonlinear process due to the periodic nature of the waveguides. However, the QPM condition is satisfied by using a right combination of the tapering period and modulation amplitude that allow an alignment between the Fourier spectra of the nonlinear coefficient and the phase-mismatching term. Simulations show an enhancement of the TH conversion efficiency by 50 dB after 1000 periods of propagation. Finally, I envisage that this work will stimulate and open new areas of research. In fact, it could revolutionize the applications of integrated nonlinear optics using materials, such as silicon or other CMOS-compatible compounds that are incompatible with periodically poled techniques.

ACKNOWLEDGMENTS

The author thanks Prof. A. Mussot and Dr. A. Kudlinski at the University of Lille in France, as well as Dr. F. Biancalana, Dr. A. Fedrizzi, and Prof. R. Thomson at Heriot-Watt University in the UK for useful discussions. The author also acknowledges the support of his research by Royal Society of Edinburgh (RSE).

[1] B. E. A. Saleh and M. C. Teich, *Fundamentals of Photonics*, 2nd ed. (Wiley, New York, 2007).
[2] D. A. Kleinman, Phys. Rev. **128**, 1761 (1962).
[3] J. A. Armstrong, N. Bloembergen, J. Ducuing, and P. S. Pershan, Phys. Rev. **127**, 1918 (1962).
[4] D. Feng, N.-B. Ming, J.-F. Hong, Y.-S. Yang, J.-S. Zhu, Z. Yang, and Y.-N. Wang, Appl. Phys. Lett. **37**, 607 (1980).
[5] M. M. Fejer, G. A. Magel, D. H. Jundt, and R. L. Byer, IEEE J. Quantum Electron. **28**, 2631 (1992).
[6] X. P. Hu, P. Xu, and S. N. Zhu, Photon. Res. **1**, 171 (2013).
[7] S. Tanzilli, H. D. Riedmatten, H. Tittel, H. Zbinden, P. Baldi, M. D. Micheli, D. B. Ostrowsky, and N. Gisin, Electron. Lett. **37**, 26 (2001).
[8] A. Dosseva, L. Cincio, and A. M. Brańczyk, Phys. Rev. A **93**, 013801 (2016).
[9] G. P. Agrawal, *Nonlinear Fiber Optics*, 4th ed. (Academic Press, San Diego, CA, 2007).
[10] J. E. Sharping, K. F. Lee, M. A. Foster, A. C. Turner, B. S. Schmidt, M. Lipson, A. L. Gaeta, and P. Kumar, Opt. Express **14**, 12388 (2006).
[11] J. Fulconis, O. Alibart, J. L. O'Brien, W. J. Wadsworth, and J. G. Rarity, Phys. Rev. Lett. **99**, 120501 (2007).
[12] H. Takesue, H. Fukuda, T. Tsuchizawa, T. Watanabe, K. Yamada, Y. Tokura, and S. ichi Itabashi, Opt. Express **16**, 5721 (2008).
[13] A. Efimov, A. J. Taylor, F. G. Omenetto, J. C. Knight, W. J. Wadsworth, and P. S. J. Russell, Opt. Express **11**, 2567 (2003).
[14] M. Corona, K. Garay-Palmett, and A. B. U'Ren, Phys. Rev. A **84**, 033823 (2011).
[15] M. G. Moebius, F. Herrera, S. Griesse-Nascimento, O. Reshef, C. C. Evans, G. G. Guerreschi, A. Aspuru-Guzik, and E. Mazur, Opt. Express **24**, 9932 (2016).
[16] A. Cavanna, F. Just, X. Jiang, G. Leuchs, M. V. Chekhova, P. S. Russell, and N. Y. Joly, Optica **3**, 952 (2016).
[17] B. Corcoran, C. Monat, C. Grillet, D. J. Moss, B. J. Eggleton, T. P. White, L. O'Faolain, and T. F. Krauss, Nat. Photon. **3**, 206 (2009).
[18] M. Hillery, V. Bužek, and A. Berthiaume, Phys. Rev. A **59**, 1829 (1999).
[19] A. M. Lance, T. Symul, W. P. Bowen, B. C. Sanders, and P. K. Lam, Phys. Rev. Lett. **92**, 177903 (2004).
[20] T. Rudolph, APL Photonics **2**, 030901 (2017).
[21] J. Kim, O. Boyraz, J. H. Lim, and M. N. Islam, J. Lightwave Technol. **19**, 247 (2001).
[22] U. K. Sapaev, I. Babushkin, and J. Herrmann, Opt. Express **20**, 22753 (2012).
[23] X. Jiang, T. Lee, J. He, M. I. M. A. Khudus, and G. Brambilla, Opt. Express **25**, 22626 (2017).
[24] K. Tarnowski, B. Kibler, C. Finot, and W. Urbanczyk, IEEE J. Quant. Electron. **47**, 622 (2011).
[25] J. B. Driscoll, N. Ophir, R. R. Grote, J. I. Dadap, N. C. Panoiu, K. Bergman, and R. M. Osgood, Opt. Express **20**, 9227 (2012).
[26] M. Droques, A. Kudlinski, G. Bouwmans, G. Martinelli, and A. Mussot, Opt. Lett. **37**, 4832 (2012).
[27] M. Droques, A. Kudlinski, G. Bouwmans, G. Martinelli, and A. Mussot, Phys. Rev. A **87**, 013813 (2013).
[28] S. R. Nodari, M. Conforti, G. Dujardin, A. Kudlinski, A. Mussot, S. Trillo, and S. De Bièvre, Phys. Rev. A **92**, 013810 (2015).
[29] F. Copie, A. Kudlinski, M. Conforti, G. Martinelli, and A. Mussot, Opt. Express **23**, 3869 (2015).
[30] R. Stolen and J. Bjorkholm, IEEE J. Quant. Electron. **18**, 1062 (1982).

[31] J. D. Love, W. M. Henry, W. J. Stewart, R. J. Black, S. Lacroix, and F. Gonthier, IEEE Proc. J. Optoelectron. **138**, 343 (1991).
[32] S. Yerolatsitis, I. Gris-Sánchez, and T. A. Birks, Opt. Express **22**, 608 (2014).
[33] K. M. Davis, K. Miura, N. Sugimoto, and K. Hirao, Opt. Lett. **21**, 1729 (1996).
[34] M. Belt, M. L. Davenport, J. E. Bowers, and D. J. Blumenthal, Optica **4**, 532 (2017).
[35] J. Jasny, B. Nickel, and P. Borowicz, J. Opt. Soc. Am. B **21**, 729 (2004).
[36] D. B. Leviton and B. J. Frey, Proc. SPIE **6273**, 62732K (2006).